Photochemical & Photobiological Sciences (2021) 20:985–996
https://doi.org/10.1007/s43630-021-00066-2

ORIGINAL PAPERS

Aerosol-based antimicrobial photoinactivation in the lungs: an action spectrum study

Chiara Treghini[1] · Alfonso Dell'Accio[1] · Franco Fusi[1] · Giovanni Romano[1]

Received: 4 December 2020 / Accepted: 15 June 2021 / Published online: 17 July 2021

Abstract
Chronic lung infections are among the most diffused human infections, being often associated with multidrug-resistant bacteria. In this framework, the European project "Light4Lungs" aims at synthesizing and testing an inhalable light source to control lung infections by antimicrobial photoinactivation (aPDI), addressing endogenous photosensitizers only (porphyrins) in the representative case of *S. aureus* and *P. aeruginosa*. In the search for the best emission characteristics for the aerosolized light source, this work defines and calculates the photo-killing action spectrum for lung aPDI in the exemplary case of cystic fibrosis. This was obtained by applying a semi-theoretical modelling with Monte Carlo simulations, according to previously published methodology related to stomach infections and applied to the infected trachea, bronchi, bronchioles and alveoli. In each of these regions, the two low and high oxygen concentration cases were considered to account for the variability of in vivo conditions, together with the presence of endogenous porphyrins and other relevant absorbers/diffusers inside the illuminated biofilm/mucous layer. Furthermore, an a priori method to obtain the "best illumination wavelengths" was defined, starting from maximizing porphyrin and light absorption at any depth. The obtained action spectrum is peaked at 394 nm and mostly follows porphyrin extinction coefficient behavior. This is confirmed by the results from the best illumination wavelengths, which reinforces the robustness of our approach. These results can offer important indications for the synthesis of the aerosolized light source and definition of its most effective emission spectrum, suggesting a flexible platform to be considered in further applications.

Keywords Antimicrobial photoinactivation · Chronic lung infections · Photo-killing action spectrum · Monte Carlo simulation · *Pseudomonas aeruginosa* · *Staphylococcus aureus*

1 Introduction

In the context of antibiotic resistance (ABR), lung chronic infections are among the most affected worldwide [1–3]. For example, *Pseudomonas aeruginosa* infection is the leading cause of morbidity and mortality in cystic fibrosis patients, while methicillin-resistant *Staphylococcus Aureus* is among the hospital-acquired chronic and acute lung infection with most clinical interest [4]. The only available treatment for these infections is the use antibiotics, inhalable compounds being favoured over systemic ones mainly due to their higher deposition ratio at the site of the infection [5]. Current antibiotics are insufficiently effective because of their wide use which often induces ABR and for the presence of bacterial biofilm which represents their defence strategy against antibiotics [6].

In this context, both antimicrobial PDT (aPDT) and aPDI can play an important role in overcoming ABR, with or without the use of external photosensitizers and/or the contemporary use of antimicrobial compounds [7–9]. In human applications of aPDT, most results are either related to in vitro or ex vivo proof-of-principle experiments or concern the in vivo treatment of external organs, such as the case of skin and mucosal infections [10] due also to the relative facility in designing and using illumination sources. PDT clinical applications in the case of internal organ diseases is

Chiara Treghini and Alfonso Dell'Accio have equally contributed to this work.

✉ Franco Fusi
franco.fusi@unifi.it

[1] Department of Experimental and Clinical Biomedical Sciences "Mario Serio", University of Florence, viale Pieraccini 6, 50139 Florence, Italy

increasingly growing, even if the vast majority of applications are in the antitumor field [11].

In the case of the lungs, research has been concentrating in antitumor PDT since long time [12], results about aPDT applications being relatively more recent [13–16]. In the case of PDT, we cannot exclude the presence of external photosensitizers (PS). Differently, in aPDI, the therapy is based only on endogenous PS in the form of bacterial porphyrins; of course, the therapeutic outcome would be much increased by the presence of external PS, this having a downside associated in particular to the requirement of specificity and the introduction of a pharmacologic treatment instead of a light-treatment only. Even if most bacteria are known to contain porphyrins [17], many good photo-killing results have been obtained on few species and in particular *S. aureus* and *P. aeruginosa,* whose intrinsic photosensitivity is well known to the scientific community [18], even if the biofilm they produce as the pathogenesis progresses introduces a difficulty for the success of the phototherapeutic approach [19].

In any case, both aPDT and aPDI suffer intrinsically from the difficulty in illuminating all the pathology-affected regions (e.g. bronchi, alveoli), which depend on the pathology and its grade and development in time. Till now, solutions for therapeutic light delivery in the lungs have considered the use of modified bronchoscopes and optical fibers [13, 16] and external illumination [20], always in combination with exogenous photosensitizers [21]. Very few works report phantom or ex vivo studies to design illumination schemes for therapeutic purpose [14], the majority of them analysing diagnostic illumination schemes.

In this context, the *Light4Lungs* European project aims to define, synthesize and evaluate the efficacy of an inhalable light source in the form of a light-emitting phosphorescent aerosol, to contain chronic lung infections associated to *S. aureus* and/or *P. aeruginosa*, without external PS to increase the minimally invasive character of the proposed therapeutic scheme. The emission characteristics of the aerosol particles have to be carefully planned, to exploit every emitted photon in the best way. In addition to the emission lifetime, in the 5–30 s timespan, one of the most important requirements is the optimization of the photo-killing efficacy against the chosen representative species (*S. aureus*, *P. aeruginosa*), taking into account the presence of biofilm on the lumen wall of the lung airways. Focusing our attention to the representative case of cystic fibrosis patients, all lung regions can in principle be affected by the associated infections (trachea, bronchi, bronchioles and alveoli, see for example [22]) but at the same time all regions can be reached by light via the aerosol, provided the chemo-physical characteristics of the aerosol particles are properly defined and obtained. This a priori possibility to target with light all lung regions is in itself a great advantage, which could be exploited beyond the case of cystic fibrosis. This aspect further justifies the choice to include all lung regions in our model.

To take advantage of all the emitted photons, light therapeutic efficacy has to be maximized, bearing in mind the geometry and physics of light interaction with the biofilm and the mucous (BM layer) and, possibly, the underlying tissues. Therefore, a careful analysis of light–bacteria interaction in the infected lung environment can provide important information about the required emission spectrum for the aerosol particles.

To this aim, this communication proposes a method to find the action spectrum for bacteria photo-killing in the above-described conditions, relying on endogenous PS only. The aerosol was modelled by a homogeneous and diffuse light source inside the airways, illuminating the BM layer deposited onto the wall of the airway lumen and inside the alveoli, regardless of the specific and preferential localization of the aerosol in a real specific case. This, in fact, depends on many factors (chemo-physics of the aerosol particles, aerosolization process, aerosol intake protocol, airways conditions) and is beyond the scope of this article; it has to be considered that in any situation, the aerosol will be always localized in the entire lung, still being it possible to predict (or measure) its repartition among the various regions.

On the other hand, light–BM layer interaction was modelled applying the same method used for previous publication on the photo-killing action spectrum in the stomach [23]. Monte Carlo simulations were performed following geometrical modelling and analysis of the relevant optical parameters taken from the literature. Final results were compared with a second method, defining the best illumination spectrum and starting from optimization of bacteria porphyrin absorption within the BM layer. The obtained curves were then compared with porphyrin absorption coefficient and analysed to derive indications for the spectrum of the aerosol particle emitters.

2 Experimental

2.1 Pathological conditions and anatomo-functional model

The pathological conditions considered in this study correspond to those correlated with cystic fibrosis, which is associated with the presence of either *P. aeruginosa* or *S. aureus* species (or both) in the form of biofilm. In the perspective of studying light–tissue interaction by use of the luminous aerosol, this pathologic condition was modelled, in the following regions of the bronchial tree: trachea, bronchi, bronchioles and alveoli, which were considered representative of the aerosol-based therapeutic approach;

the related anatomo-pathological data were obtained from the literature [24–26]. Following the illumination scheme depicted in Fig. 1, the first light target was represented as a homogeneous layer of mixed biofilm and mucous components (the BM layer) containing both species of *P. aeruginosa* and *S. aureus*. In this model, the "mixing" described above refers to the definition of a layer whose mass density, bacteria numerical density, light absorber density and optical properties are constant in every point and defined as described in the next sections. Being interested in the interaction of photons within the BM layer only, this model neglects the presence of the underlying tissue (epithelium, cartilage, connective tissue). From an optical point of view, this corresponds to neglecting the contribution of reflected and back-scattered photons at the interface between the BM layer and the epithelium.

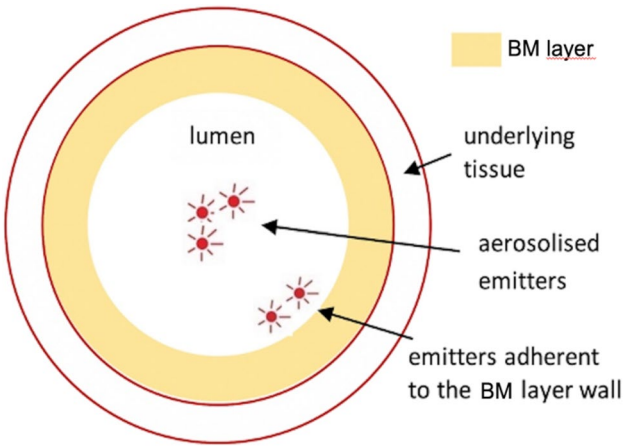

Fig. 1 Schematic model of the aerosol-based illumination of the lung airways. Therapeutic photons are emitted from the lumen volume and surface, encountering the BM layer first, then the underlying tissue

To account for the variability of in vivo conditions, in each of the aforementioned lung regions two different cases were considered i.e. low and high $[O_2]$ (oxygen concentration) conditions for the BM layer. In general, these correspond to different BM layer thickness and porphyrin concentration values and were simulated by varying these parameters according to the literature data [27–30] while mucous composition was not varied. In particular, porphyrin concentration is reported to depend on $[O_2]$ due to metabolic adaptation reasons [31]. In our modelling scheme, therefore, the two low/high $[O_2]$ cases have been associated to two different and representative porphyrin concentrations as reported in Table 1.

BM layer mean thickness in low $[O_2]$ conditions was derived from literature data about *P. aeruginosa* biofilm thickness in vitro and biofilm + mucous thickness measured in cystic fibrosis patients [8, 25]. In particular, BM layer thickness in high $[O_2]$ conditions was estimated by adding bacterial biofilm thickness in vitro [8, 32] to the mucous thickness in a normal (non-pathologic) patient [25]. In the following table, we resume the modelled conditions for

Table 1 BM layer characteristics showed in a and b

(a) BM layer characteristics for all regions and conditions

Absorption	Scattering	Refractive index	Absorber and bacteria concentration with depth
Water [46], Mucin [47], PPIX (https://omlc.org), Coproporphyrin [33], Uroporphyrin [34], Pyocyanin [35], Carotenoids [36]	10% Intralipid® [39]	$n = n_{water}$	Constant

(b) BM layer peculiar characteristics according to the specific region and condition

Region	Condition		
	Characteristics	High $[O_2]$	Low $[O_2]$
Trachea/Bronchi	Mean thickness	52 µm	500 µm
	Bacteria density	10^8 CFU/ml	10^8 CFU/ml
	Porphyrin concentration	$1.06 \cdot 10^{-8}$ M	$7.56 \cdot 10^{-8}$ M
	Oxygen gradient	230–160 µM	230–10 µM
Bronchioles	Mean thickness	43 µm	300 µm
	Bacteria density	10^8 CFU/ml	10^8 CFU/ml
	Porphyrin concentration	$1.06 \cdot 10^{-8}$ M	$7.56 \cdot 10^{-8}$ M
	Oxygen gradient	230–170 µM	230–33 µM
Alveoli	Mean thickness	40 µm	100 µm
	Bacteria density	10^8 CFU/ml	10^8 CFU/ml
	Porphyrin concentration	$1.06 \cdot 10^{-8}$ M	$7.56 \cdot 10^{-8}$ M
	Oxygen gradient	230–170 µM	230–120 µM

each region and for both the high [O_2] and low [O_2] cases. The list of the representative species characterizing the BM layer absorption properties is the following: water, mucin (from mucous), protoporphyrin IX (PPIX) (https://omlc.org), coproporphyrin [33] and uroporphyrin [34], pyocyanin (from *P. aeruginosa*) [35], carotenoids (from *S. aureus*) [36]. In particular, in all conditions and regions mucin concentration has been defined to be 5% [37], while the porphyrin types and their relative concentration have been evaluated as a function of both the bacteria species and the presence of low / high [O_2] as described before. The in vivo CFU concentration for both *P. aeruginosa* and *S. aureus* was taken from literature data [24, 38] and considered the same for both species.

On the other side, the BM layer scattering properties were modelled by considering the measured scattering coefficient of the Intralipid® colloid [39] (see also next section). In fact, Intralipid® is a lipid emulsion used e.g. in parenteral nutrition, which is widely considered as a testing scattering medium for tissue phantom generation.

2.2 Optical properties

Before performing the Monte Carlo simulations, we first calculated the BM layer optical properties for each region and condition in terms of refractive index (n) and absorption, scattering and anisotropy coefficients ($\mu_a(\lambda)$, $\mu_s(\lambda)$, $g(\lambda)$, respectively).

In particular, μ_a was obtained following the Lambert–Beer law for an absorbing medium containing multiple species:

$$\mu_a(\lambda) = \sum_i \mu_{ai}(\lambda) = \sum_i \varepsilon_i(\lambda) c_i ln10, \tag{1}$$

where μ_{ai} is the absorption coefficient of the i-th species, ε_i and c_i are the extinction coefficient and molar concentration of the i-th species, respectively (see Table 1 for the list of the absorbing species).

As anticipated, the values for $\mu_s(\lambda)$ and $g(\lambda)$ were taken from literature [39]. For all cases, in the absence of specific information regarding the variability of the scattering coefficient of the BM layer with the lung region and/or the presence of aerobic/anaerobic conditions. Finally, the BM layer refractive index was approximated to that of pure water [40].

2.3 Action spectrum

Following the methodology present in other studies [23], the action spectrum for bacterial photo-killing for each chosen condition and region can be defined as:

$$K(\lambda) = T(\lambda)\, \epsilon(\lambda)\, \phi(\lambda), \tag{2}$$

where $T(\lambda)$ is the transmittance of a D_{eff}-thick layer, representing an *effective* thickness for the BM layer, as detailed in the following; $\varepsilon(\lambda)$ is the porphyrin molar extinction coefficient, defined as an averaged mean over their relative concentration; $\varphi(\lambda)$ is the porphyrin quantum yield for ROS production [41]. To obtain $T(\lambda)$, for each chosen region ("bigger" bronchi, "smaller" bronchi, alveoli) the problem is restricted to a one-dimensional model, with a two-step approach:

Step 1: reduction of the initial 3D problem into a one-dimensional model and definition of an effective thickness D_{eff} for the BM layer in the specific region (trachea, bigger bronchi, smaller bronchi, alveoli) and condition (high [O_2]/low [O_2]). This is depicted in Fig. 2, where the first line refers to the case of trachea, bigger and smaller bronchi, which have the same cylindrical geometry; the second line refers to the alveoli case and the third bottom line refers to the one-dimensional reduction of the problem and definition of the problem geometry.

Following the methodology present in previous studies [23], D_{eff} was obtained in three steps. First, we analysed the problem geometry (cylindrical for trachea, bronchi and bronchioles, spherical for alveoli) and obtained d_{max} as a function of the incidence angle (α in Fig. 2) in a planar geometry that simplifies the more complex 3D geometrical problem (see Fig. 2). This hypothesis was justified in retrospect, as explained below.

Then, d_{eff} (α) was obtained by means of a weighted mean of the depth inside the BM layer (x in Eq. 3) in the range 0–d_{max}(α):

$$d_{eff}(\alpha) = \frac{\int_0^{d_{max}(\alpha)} x e^{-\mu x}\, dx}{\int_0^{d_{max}(\alpha)} e^{-\mu x}\, dx}, \tag{3}$$

where $1/\mu$ is the average light penetration depth in the BM layer. The weighting factor $e^{-\mu x}$ represents the Lambert–Beer exponential decrease of light power and, therefore, the consequent decrease in bacteria photokilling efficacy.

In Eq. 3, μ was derived according to Eq. (1), while d_{max} was calculated by a geometrical modelling of the specific region conditions (see Fig. 2). Finally, D_{eff} was obtained by averaging d_{eff} (α) over the incidence angle α:

$$D_{eff} = \frac{1}{\pi/2} \int_0^{\pi/2} d_{eff}(\alpha) d\alpha. \tag{4}$$

Step 2: perform a Monte Carlo simulation on a D_{eff}-thick BM layer to obtain $T(\lambda)$, as detailed below. In general, a purely analytical approach to the calculation of d_{max} (α) and d_{eff} (α) is very complex if the BM layer 3D structure is explicitly considered, as it would imply the dependence of those quantities on additional degrees of freedom. This

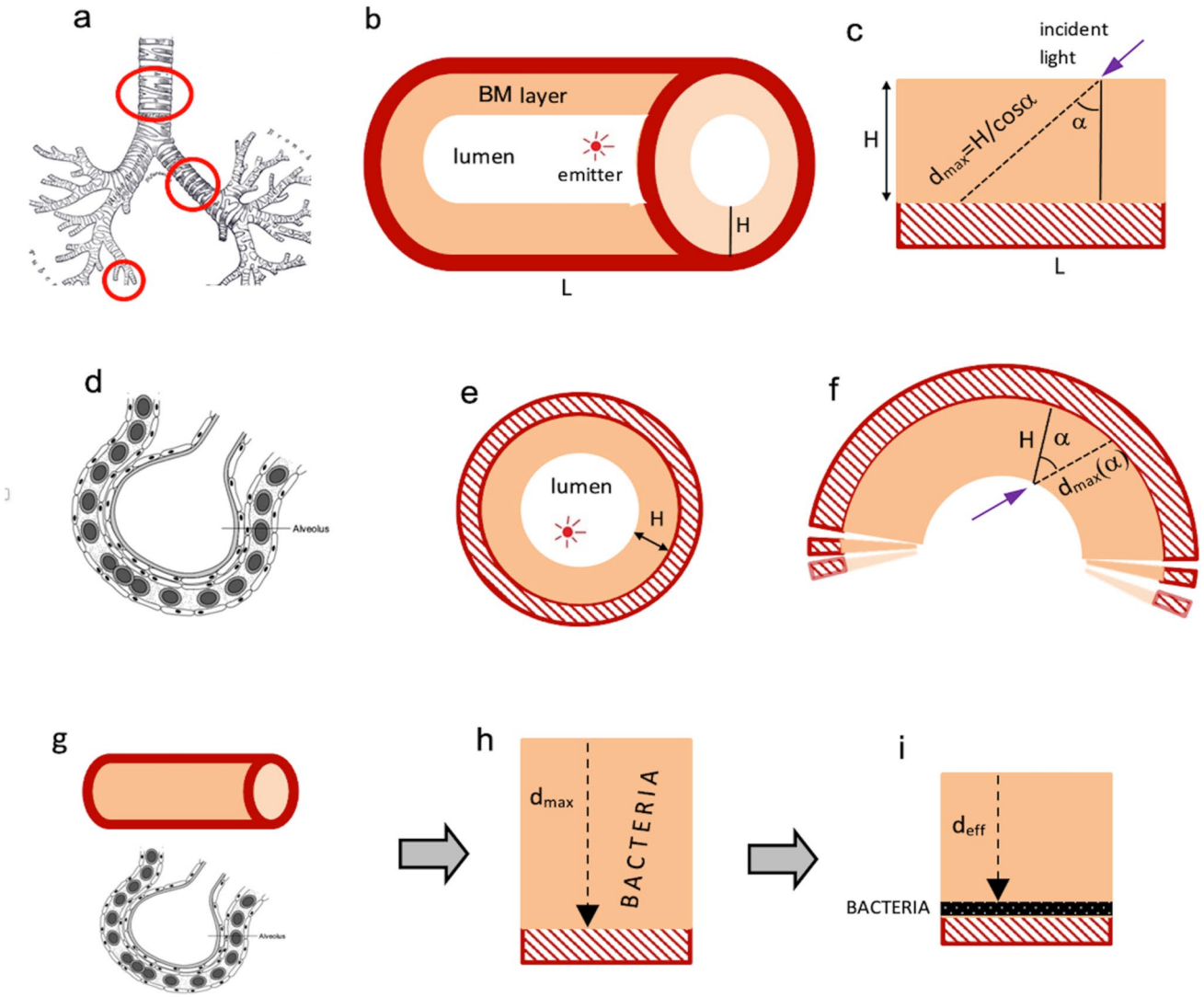

Fig. 2 Modelling of representative lung regions. First line: representation of the cylindric geometry for trachea, bronchi and bronchioles (**a**, **b**); definition of the d_{max} parameter as a function of the illumination geometry in every point of the BM layer surface (**c**). Second line: representation of a spherical geometry for alveoli (**d**, **e**); definition of d_{max} as a function of the illumination geometry (**f**). Third line: definition of d_{max} as a mean over the illuminated surface by representation of the equivalent unidimensional case (**g**, **h**); definition of D_{eff} (**i**)

would be associated to the "exact" calculation of d_{max} and d_{eff}, then of D_{eff}. The maximum difference respect to our calculated values for D_{eff} was estimated to be of about 10% for all regions (data not shown), with very acceptable consequences on the final estimated value for the action spectrum (see section on error analysis).

2.4 Monte Carlo simulation

The Monte Carlo simulation was used to obtain $T(\lambda)$ (Eq. 2) and also for successive analysis to obtain the "best illumination spectrum", as described below. The simulation was performed using the MCML free software [42] and purposely made data-analysis routines (MatLab v.R2020A and Microsoft Excel 2020). The software defines a vertically impinging photon flux; in our case we considered the following photon-related parameters for the simulation: wavelength range 380–700 nm, being $\Delta\lambda = 1$ nm between two successive wavelengths; 10^6 photons per chosen wavelength. Photons were considered to be incident from air into a homogeneous medium representing the BM layer.

2.5 Best illumination wavelengths

To have a confirmation of the robustness of the method used to obtain the action spectrum, we developed a methodology to calculate the "best illumination wavelength", defined as the one maximizing bacterial porphyrin excitation in our

modelled conditions. This definition is intrinsically arbitrary, being possibly substituted by other definitions that explicitly consider the consequent formation of ROS and/or bacterial cell photo-killing efficacy. Nevertheless, in this context we preferred to stop at the stage of PS excitation, leaving considerations on the biological consequences to future work.

In the following, we start from considering the desired photon wavelength and number at each depth z_i inside the BM layer, and consequently derive the desired characteristics of the impinging light in terms of wavelength(s) and photon number. Referring to Fig. 3, let us divide our problem into two steps, where we define the wavelength (λ_{best}) and number of photons (n_{best}) maximizing porphyrin excitation in a volume ΔV inside the BM layer containing n_p porphyrin molecules, being n_{best} intended as the minimum photon number associated to that purpose:

Case 1) n_p porphyrins at $z=0$:

λ_{best} = peak wavelength of the function $\varepsilon(\lambda)$ for all photons and $n_{best} = n_p / \varepsilon(\lambda_{best})$.

This choice maximizes the excitation probability, considering that no photon absorption is present before interaction with the porphyrins.

Case 2) n_p porphyrins in the layer between z_i and $z_i + \Delta z$, with $0 < z_i \leq H$:

λ_{best} = peak wavelength of the function $\varepsilon'(\lambda) = \varepsilon(\lambda)\, T(\lambda_{best}, z)$ for all photons and $n_{best} = n_p/(\varepsilon(\lambda_{best})\, T(\lambda_{best}, z))$ where $T(\lambda_{best}, z)$ comes from the Monte Carlo Simulation. It is worth noticing that this choice accounts for the presence of both absorption and scattering of all the BM layer above the porphyrin depth, there included porphyrin absorption itself. Respect to case 1, here we have to further raise the photon number arriving at depth = z by taking into account photon extinction due to a z-deep BM layer.

By repeating this method for any depth up to $z=H$, we can build a discrete impinging light spectrum $S_i = S(\lambda_i)$ where $i = 1, \ldots, N$ numbers the BM layers of equal thickness Δz ($i=1$ being the top one), λ_i and $n_i = n(\lambda_i)$ being equal to λ_{best} and n_{best} for the i-th layer, respectively.

2.6 Error analysis

Errors in obtaining the action spectrum and the best excitation wavelengths were associated to the reproducibility of the obtained results.

Starting from the very many variables involved, we analysed the variation of the action spectrum as a function of the chemo-physical and optical parameters as well as the geometrical ones:

(i) bacterial porphyrin concentration (from: modelling of the pathological conditions);
(ii) geometry parameters (from: modelling of the pathological lung anatomy, e. g. BM layer thickness);
(iii) optical characteristics of the absorbers e.g. μ_a e μ_s;
(iv) D_{eff}, associated to the methodology to reduce the problem to a mono-dimensional one.

All these parameters have been used, directly or indirectly, to calculate the action spectrum K (λ) (Eq. 2). Due to its key role in representing the problem geometry and for performing the Monte Carlo simulation, D_{eff} was considered as the main parameter whose variation summarized the presence of multiple errors in the overall method. The dependence of the action spectrum curve on D_{eff} was tested by imposing an arbitrary but reasonable variation of ± 10% on the D_{eff} value, representative of the overall error on its determination. Here, two different analysis were performed:

(i) variation in the action spectrum shape, i.e. in K (λ) curves for $D_{eff\ best}$ and $D_{eff\ best}$ ±10%, all normalized at their respective maximum;
(ii) variation in the action spectrum curve values respect to the best case, i.e. analysis of the 3 curves K_{best} = K (λ, $D_{eff\ best}$), K+ = (λ, $D_{eff\ best}$ +10%), K– = K (λ, $D_{eff\ best}$ -10%).

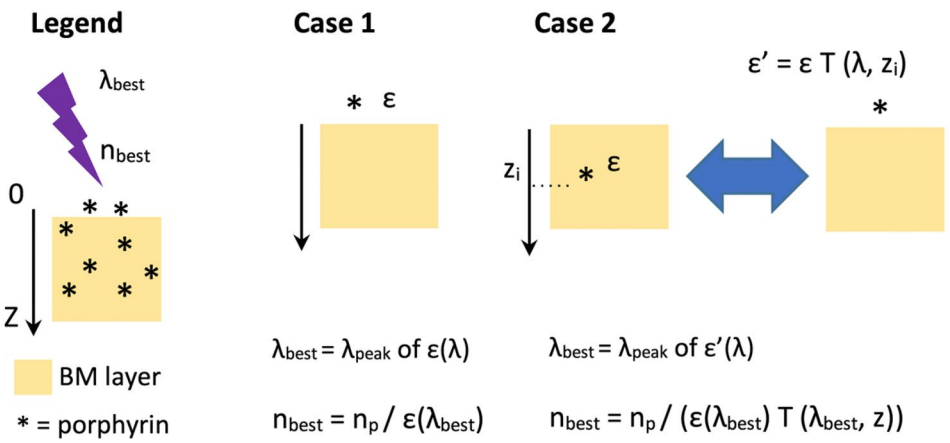

Fig. 3 Scheme representing the model used to define the best excitation light spectrum for endogenous bacteria porphyrins in the BM layer. n_p is the number of porphyrins in each Δz layer at depth z_i

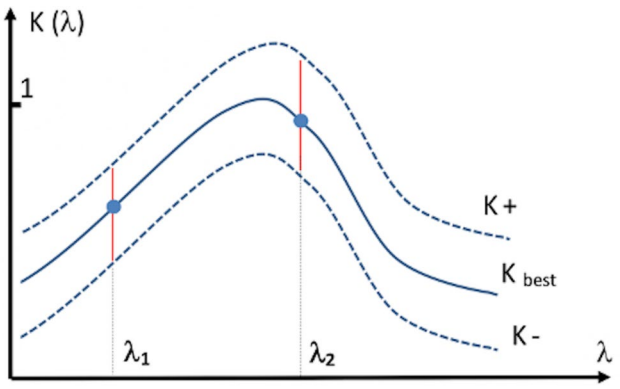

Fig. 4 Scheme depicting the influence of action spectrum variability on the determination of the relative efficacy of two generic wavelengths λ_1 and λ_2

In particular, case (ii) is important when comparing action spectrum values at 2 different wavelengths. Referring to the generic representative scheme shown in Fig. 4, the relative photokilling efficacy at λ_1 respect to λ_2 is represented by the ratio $K_{best}(\lambda_1)/K_{best}(\lambda_2)$, which in turn depends on the variability ("error") depicted by the vertical segments in correspondence of λ_1 and λ_2, respectively, and suggesting an error propagation procedure. In addition, the influence of the concentration parameters on the BM layer transmittance was tested, by imposing a separate ± 10% variation in μ_a and μ_s respectively and testing its influence on K (λ).

Due to the primary role of endogenous porphyrins in aPDI, their concentration was varied of ± 1 order of magnitude respect to the chosen representative value (Table 1), maintaining all the other parameters constant. This choice is justified by the variability in the bacterial CFU counts/ml found in literature studies. The action spectrum curves were correspondingly obtained.

Finally, the light irradiance reflected back into the BM layer by the underlying tissue (E_R) was first estimated in terms of expected mean reflectance R. This was done by applying the Fresnel equations at the interface between the BM layer and the successive tissue, limiting our analysis to the normal incidence case. To apply the simplified Fresnel equation, we considered $n = 1.33$ for the BM layer and $n = 1.37$ [43] for the underlying tissue. Starting from R, the ratio between E_R and the irradiance at the lumen side of the BM layer ("impinging irradiance") was also estimated.

3 Result and discussion

3.1 D_{eff} values

The results for the D_{eff} values are resumed in Table 2. These values reflect in part the dimensions of the different lung regions; better, we should consider that the mean operation over the geometrical variables defining d_{max} gives similar results for different lung regions, namely trachea, bronchi and bronchioles. This is due to the longitudinal and transversal dimensions (L and S respectively, Fig. 2) being such that L > > H, considering that mean values for L are in the 1.3 cm range for bronchioles and 5–12 cm for bronchi and trachea [44].

Table 2 D_{eff} values, shown for the *P. aeruginosa* case

	D_{eff} values (μm)			
	Trachea	Bronchi	Bronchioles	Alveoli
Low $[O_2]$	232	212	184	53
High $[O_2]$	61	57	53	57

Results for the case of *S. aureus* are substantially coincident within few percent (e.g. 186 μm for the bronchioles case—low $[O_2]$ conditions)

Following Eq. 3, the maximum theoretical value for D_{eff} can be obtained by considering $d_{max} = +\infty$ for all α, which gives $D_{eff} = 1/\mu \approx 290$ μm for both cases, being $\mu = 34.6\ cm^{-1}$ and $34.2\ cm^{-1}$ for *P. aeruginosa* and *S. aureus*, respectively.

In general, in fact, the exponentially decreasing behaviour of the weighting factor (see Eq. 2 and 20) defining D_{eff}, mitigates its dependence on the geometrical parameters, which in turn results in a small variation of the normalized action spectrum curve. In other words, sensitive relative variations in d_{max} (due to modelling errors or anatomical variability) do not result in sensitive variations in the final action spectrum shape.

It is worth mentioning that, unlike [23] here we have a diffused light source (a luminous aerosol), meaning that light emitters can be located in any point inside the lumen including the lumen surface. The averaging operation that defines D_{eff} is compatible with this condition but does not take into account any possible influence (if any) of a non-uniform aerosol distribution (emitter density) along the specific airway region. In other terms, our approach remains valid in the case of a non-uniform aerosol distribution provided it happens at the whole lung scale level and not on a local one, which corresponds to a realistic expectation [21].

3.2 Action spectrum

The results for the action spectrum are shown in Fig. 5a. Starting from 16 possible cases (2 bacteria types, 2 conditions, 4 regions) the normalized action spectrum curves were grouped into 4 categories (1 to 4, Table 3). The differences between these 4 curve types can be found in:

(i) a dissimilar behaviour in the 410-430 nm region;
(ii) a different value of the secondary peaks.

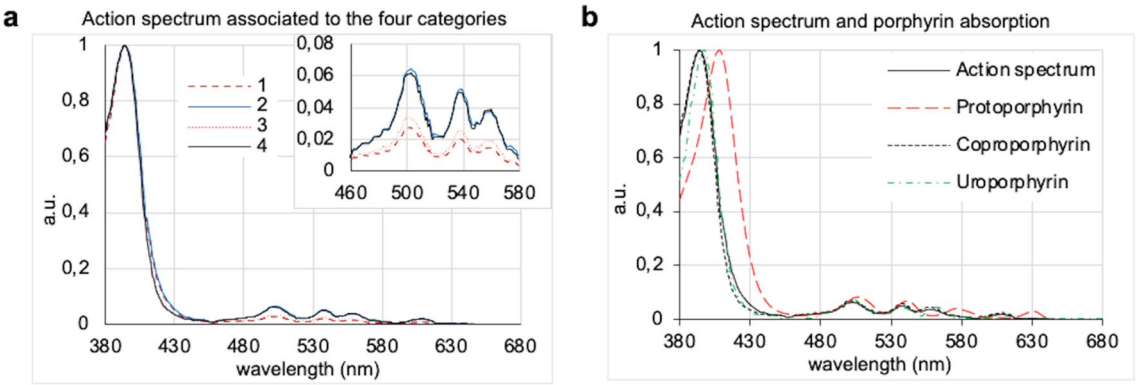

Fig. 5 Normalized action spectrum for bacterial photo-killing in the lungs. **a** Associated to the four categories (see Table 3); **b** Comparison to porphyrin absorption spectrum (action spectrum: exemplary case related to category 2—*P. aeruginosa* high [O_2] and alveoli low [O_2])

Table 3 Subdivision of bacterial models into 4 main sub-categories, distinguishing them into regions (trachea, bronchi, bronchiole and alveolus) and conditions (high [O_2]/low [O_2])

	P. aeruginosa				*S. aureus*			
	Trachea	Bronchi	Bronchioles	Alveoli	Trachea	Bronchi	Bronchioles	Alveoli
Low [O_2]	1	1	1	2	3	3	3	4
High [O_2]	2	2	2	2	4	4	4	4

Error analysis was performed in only two representative cases of *P. aeruginosa*: anaerobic trachea and aerobic alveolus

Both of these features appear to be ancillary and can be attributed to differences in e.g. porphyrin and pigment types/concentrations between *P. aeruginosa* and *S. aureus*. Possibly, the variation in secondary to primary peak ratio in types 1–3 respect to 2–4 can be considered as the most important modulation over the various cases considered, which can be useful in evaluating the possible use of additional red light in excitation.

In all cases, the action spectrum is peaked at around 395 nm for both *P. aeruginosa* and *S. aureus* cases, being it a weighted mean over uroporphyrin (~400 nm), coproporphyrin (~395 nm) and protoporphyrin (~410 nm) peaks. The most important feature of the action spectrum curves is their close similarity to the porphyrin molar extinction coefficient, as illustrated in Fig. 5b. If on one side this could seem surprising, we have to consider that the absence of strong antagonistic absorbers with peculiar absorption peaks respect to porphyrins (visible range) is a key factor that ultimately contributes to the similarity described above and overall also to the robustness of the proposed method.

In this analysis, we should enquire the role of mucin + bacteria pigments pyocyanin and carotenoids, discarding water (whose absorption is negligible in the visible over ~100–300 µm range) and considering that in a first approximation the scattering acts as an absorption enhancer. Of course, as the simulation takes into account the absorption coefficient (μ_a in Eq. 1), we have to carefully consider also the relative absorber concentration. If on one side, mucin contribution to the μ_a is substantial, nevertheless its almost constant (slightly decreasing) behaviour in the visible range does not shift the action spectrum peak from the porphyrin main peak region, still and possibly contributing to decreasing the importance of the secondary peaks in the yellow–red. On the other side, the pigments' extinction coefficients are peaked at ~300 nm for pyocyanin and ~460 nm for carotenoids but their concentration is not high enough to result in a significant contribution to the final μ_a.

3.3 Error analysis

According to the proposed methods, the K_{best}, K_+ and K_- curves have been obtained and compared for all cases. Their normalized values do not show any appreciable difference over the whole wavelength range (data not shown), which is indicative of the robustness of the method.

The comparison between the curves, normalized respect to K_{best} maximum, is shown in Fig. 6 in the exemplary cases corresponding to categories 1 and 2. Deviations respect to the K_{best} values are ± 8–18% for category 1 and ± 2–4% for category 2, considering the whole wavelength range 380–700 nm. Besides, a ± 10% variation of the optical parameters μ_a and μ_s resulted in a transmittance variation for the BM layer of about ± 5% and ± 4%, respectively, which in turn was associated to a negligible variation in the action spectrum values. Finally, the estimated back-reflected light fraction by the tissues beneath the BM layer is of about

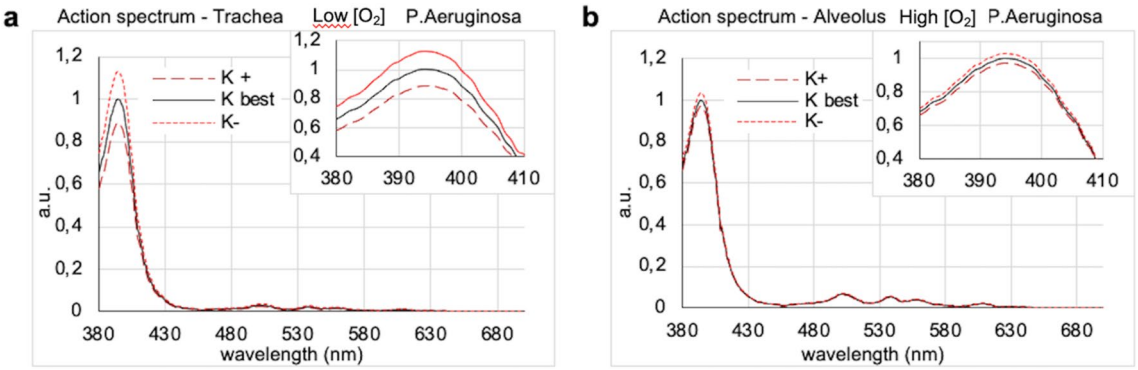

Fig. 6 Effect of D_{eff} variability on the action spectrum. **a** Cases relative to category 1 (see Table 3); **b** Cases relative to category 2

$2 \cdot 10^{-4}$. This gives in any case a negligible value ($<<1\%$) for the irradiance fraction re-entering the BM layer, respect to the irradiance incident at the lumen level.

Finally, the action spectrum curves obtained by varying the bacterial CFU/ml between 10^7 and 10^9 showed no significant variations (data not shown).

3.4 Best illumination wavelengths

In all cases, the result for best illumination wavelengths (as defined in the "Materials and methods") give the only $\lambda = 394$ nm, in accordance with the action spectrum main peak. The presence of a single wavelength (corresponding to an ideally very narrow illumination spectrum) is not surprising. In fact, the method selects only the peak wavelength of $\varepsilon'(\lambda)$ (see Fig. 3), at any depth inside the BM layer. Analysis of the $\varepsilon'(z, \lambda)$ behaviour shows that the importance of the main peak decreases with increasing depth, while secondary peaks increase but not to the point of overcoming the main one, at least for the thickness values considered in our model (data not shown).

4 Conclusions

This work is related to the development of an innovative and inhalable light source in the form of a luminous aerosol, to control lung infections associated to the presence of *S. aureus* and/or *P. aeruginosa*. As an exemplary case, we considered the anatomic-pathological conditions associated with cystic fibrosis, one of the most important targets of the proposed therapeutic approach based on aPDI in the lungs. Following previous work related to aPDI in the stomach, we started by applying the same semi-theoretical methodology to derive the in vivo action spectrum for bacterial photokilling in the lungs. The robustness of the method was tested by applying a second methodology to obtain an independent confirmation on the characteristics of the *best illumination wavelengths* optimizing endogenous PS absorption.

One of the main risks associated with minimally invasive techniques for light delivery in PDT/aPDT/aPDI is their intrinsic lack of photons or, better, lack of "intensity" definable as the irradiance at the level of the relevant tissue/anatomical region. That is why, considering a PS-free approach for exogenous compounds, we have interest in maximizing the production and efficacy of every single excitation photon. In this perspective, indications coming from the in vivo action spectrum are fundamental to optimize the therapeutic efficacy and to guide the synthesis of the best material in the form of light emitters included in the aerosolization process.

Unlike previous results for the stomach, in this case the final indications for the best excitation spectrum are in the end pretty straightforward: the action spectrum is substantially coincident with the endogenous porphyrin extinction coefficient. This difference is due to a different localization of the infection: planktonic bacteria and bacteria in biofilm are not hidden in between tissue plicae and rugae as in stomach infection by *H. pylori*, but grow onto the lumen surface of the lung airways, so that tissue optical properties have a negligible role respect to those of the BM layer. This, in turn, affects the simulation results at the basis of the proposed approach.

In fact, starting from geometrical modelling of the infected regions (trachea, bronchi, bronchioles and alveoli), we reduced the problem to one dimension only, performing Monte Carlo simulations on a homogeneous optical means representing the BM layer, having an *effective thickness* representative of the physics and geometry of light–BM layer interaction. By careful analysis of the relevant literature, scattering and absorption were accounted for including in particular the presence of mucin (from mucous), endogenous bacteria pigments and porphyrins: the main contribution to the final absorption coefficient was given by porphyrins only. This is due both to the absence of visible absorption peaks, still in the presence of a relative high concentration (the case

of mucin) and to absorption peaks being accompanied by a relatively moderate or low concentration (pigments).

These results were confirmed by the analysis of the *best illumination wavelengths*. In this case, a different methodology was used, based on a reversed attitude respect to the action spectrum one but answering to the same question. This is intrinsically not different from the classic approach to PDT, optimally illustrated by Jacques [45]. Starting from a homogeneous distribution of porphyrins in the BM layer volume, we aimed at having virtually all of them excited with maximum probability, taking into account both their extinction coefficient and the photon absorption by the BM layer itself. By considering all porphyrins at all depths, this operation builds up the "best excitation spectrum" for the light impinging at the BM layer surface. This method is fed by the knowledge of the BM layer transmittance at any depth, which was provided by the Monte Carlo simulation. Of course, this could be implemented to take into account further steps, e.g. oxygen concentration and ROS production or even link this with the desired killing effect by introducing more biology into the problem.

In conclusion, this study proposes a semi-theoretical method to obtain the action spectrum for aPDI in the lungs, emphasizing the importance of the modelling aspects and of a quantitative approach. We believe that the force of this methodology is mainly in its flexibility, as it can be applicable to any organ/tissue/region where PDT, aPDT or aPDI can be considered as a therapeutic option. Perhaps even more interesting, the flexibility is also on the possibility to afford the same problem from different perspectives: (i) to obtain the efficacy of a given source respect to another; (ii) to design the source characteristics fitting them to optimize the therapeutic efficacy of a specific case (e.g. optical fibre illumination); (iii) to find the limiting factor upon which to act primarily to exploit all the potential of a given technique.

Of course, in vitro and in vivo experiments are the natural and necessary continuation of this kind of studies.

Acknowledgements The authors thank all the other members of the Light4Lungs group for their contribution to this work: Santi Nonell, Institut Químic de Sarrià, Universitat Ramon Llull, Barcelona, Spain; Nelly Henry, Sorbonne Université, Paris, France; Emilio Palomares, Fundacio Privada Institut Catala d'Investigacio Quimica, Tarragona, Spain; Elena Reddi, University of Padova, Padova, Italy; Glyn Taylor, Cardiff Scintigraphics Ltd, Cardiff, UK; Aras Kadioglu, The University of Liverpool, Liverpool, UK. The authors thank also Alessio Gnerucci, Paola Faraoni, Silvia Calusi, University of Florence and Lucia Pallecchi, University of Siena for fruitful discussion.

Author contributions Conceptualization: CT, AD, and GR; methodology: CT; AD, and GR; formal analysis and investigation: CT and AD; writing—original draft preparation: GR; writing—review and editing: CT, AD, GR, and FF; funding acquisition: GR; supervision: FF and GR.

Funding Open access funding provided by Università degli Studi di Firenze within the CRUI-CARE Agreement. This research was supported by the project "Light4Lungs", H2020-FETOPEN-2018-2020, Grant Agreement n.863102.

Availability of data and materials Not applicable.

Code availability Software for Monte Carlo simulation is available in the website https://omlc.org/

Declarations

Conflict of interest There are no conflicts to declare.

Consent to participate All authors gave their consent to participate.

Consent for publication All authors gave their consent to publish.

Ethics approval Not applicable.

References

1. Kidd, T. J., et al. (2018). Defining antimicrobial resistance in cystic fibrosis. *Journal of Cystic Fibrosis, 17*, 696–704. https://doi.org/10.1016/j.jcf.2018.08.014
2. Nikolova, P., et al. (2013). Antibiotic resistance in ambulatory patients with chronic obstructive pulmonary disease-clinical signs. *European Respiratory Journal*, *42*, 2733.
3. Johnson, D. C. (2011). Airway mucus function and dysfunction. *New England Journal of Medicine, 364*, 978. https://doi.org/10.1056/NEJMc1014719
4. Jensen, A. G., et al. (1999). Risk factors for hospital-acquired *Staphylococcus aureus* bacteremia. *Archives of Internal Medicine, 159*, 1437–1444. https://doi.org/10.1001/archinte.159.13.1437
5. Smith, S., Rowbotham, N. J., & Regan, K. H. (2018). Inhaled anti-pseudomonal antibiotics for long-term therapy in cystic fibrosis (Review). *Cochrane Database Systematic Review.* https://doi.org/10.1002/14651858.CD001021.pub3
6. Costerton, J. W., Stewart, P. S., & Greenberg, E. P. (1999). Bacterial biofilms: A common cause of persistent infections. *Science, 284*, 1318–1322. https://doi.org/10.1126/science.284.5418.1318
7. Wainwright, M., et al. (2017). Photoantimicrobials—are we afraid of the light? *The Lancet Infectious Diseases, 17*, e49–e55. https://doi.org/10.1016/S1473-3099(16)30268-7
8. Hu, X., Huang, Y. Y., Wang, Y., Wang, X., & Hamblin, M. R. (2018). Antimicrobial photodynamic therapy to control clinically relevant biofilm infections. *Frontiers in Microbiology, 9*, 1–24. https://doi.org/10.3389/fmicb.2018.01299

9. Mulani, M. S., Kamble, E. E., Kumkar, S. N., Tawre, M. S., & Pardesi, K. R. (2019). Emerging strategies to combat ESKAPE pathogens in the era of antimicrobial resistance: A review. *Frontiers in Microbiology, 10*, 1–24. https://doi.org/10.3389/fmicb.2019.00539
10. Pérez-Laguna, V., et al. (2019). A combination of photodynamic therapy and antimicrobial compounds to treat skin and mucosal infections: A systematic review. *Photochemical and Photobiological Sciences, 18*, 1020–1029. https://doi.org/10.1039/c8pp00534f
11. Juarranz, Á., Jaén, P., Sanz-Rodríguez, F., Cuevas, J., & González, S. (2008). Photodynamic therapy of cancer. Basic principles and applications. *Clinical and Translational Oncology, 10*, 148–154. https://doi.org/10.1007/s12094-008-0172-2
12. Kato, H., et al. (2017). Review of PDT for lung cancer and future. *Photodiagnosis Photodynamic Therapy., 17*, A30–A31. https://doi.org/10.1016/j.pdpdt.2017.01.067
13. Cassidy, C. M., et al. (2011). Drug and light delivery strategies for photodynamic antimicrobial chemotherapy (PACT) of pulmonary pathogens: A pilot study. *Photodiagnosis Photodynamic Therapy., 8*, 1–6. https://doi.org/10.1016/j.pdpdt.2010.12.007
14. Durkee, M. S. (2018). Optical model of the murine lung to optimize pulmonary illumination. *Journal of Biomedial Optics, 23*, 1. https://doi.org/10.1117/1.jbo.23.7.071208
15. Musani, A. I., Veir, J. K., Huang, Z., Lei, T., Groshong, S., & Worley, D. (2018). Photodynamic therapy via navigational bronchoscopy for peripheral lung cancer in dogs. *Lasers in Surgery and Medicine., 50*, 483–490. https://doi.org/10.1002/lsm.22781
16. Zhao, Y., et al. (2019). Bioinspired heteromultivalent ligand-decorated nanotherapeutic for enhanced photothermal and photodynamic therapy of antibiotic-resistant bacterial Pneumonia. *ACS Applied Materials & Interfaces, 11*, 39648–39661. https://doi.org/10.1021/acsami.9b15118
17. Choby, J. E., & Skaar, E. P. (2016). Heme synthesis and acquisition in bacterial pathogens. *Journal of Molecular Biology, 428*, 3408–3428. https://doi.org/10.1016/j.jmb.2016.03.018
18. Amos-Tautua, B. M., Songca, S. P., & Oluwafemi, O. S. (2019). Application of porphyrins in antibacterial photodynamic therapy. *Molecules, 24*, 2456. https://doi.org/10.3390/molecules24132456
19. Taraszkiewicz, A., Fila, G., Grinholc, M., & Nakonieczna, J. (2013). Innovative strategies to overcome biofilm resistance. *BioMed Research International, 2013*, 1–13. https://doi.org/10.1155/2013/150653
20. Geralde, M. C., et al. (2017). Pneumonia treatment by photodynamic therapy with extracorporeal illumination - an experimental model. *Physiological Reports, 5*, 1–7. https://doi.org/10.14814/phy2.13190
21. Usuda, J., et al. (2006). Photodynamic therapy (PDT) for lung cancers. *Journal of Thoracic Oncology, 1*, 489–493. https://doi.org/10.1016/S1556-0864(15)31616-6
22. Bonestroo, H. J., de Winter-de Groot, K. M., van der Ent, C. K., & Arets, H. G. (2010). Upper and lower airway cultures in children with cystic fibrosis: Do not neglect the upper airways. *Journal of Cystic Fibrosis, 9*(2), 130–134.
23. Gnerucci, A., Faraoni, P., Calusi, S., Fusi, F., & Romano, G. (2020). Influence of stomach mucosa tissue on the efficacy of intragastric antibacterial PDT. *Photochemical and Photobiological Science., 19*, 34–39. https://doi.org/10.1039/c9pp00315k
24. Cowley, E. S., Kopf, S. H., Lariviere, A., Ziebis, W., & Newman, D. K. (2015). Pediatric cystic fibrosis sputum can be chemically dynamic, anoxic, and extremely reduced due to hydrogen sulfide formation. *MBio, 6*, 1–15. https://doi.org/10.1128/mBio.00767-15
25. García-Díaz, M., Birch, D., Wan, F., & Nielsen, H. M. (2018). The role of mucus as an invisible cloak to transepithelial drug delivery by nanoparticles. *Advanced Drug Delivery Reviews, 124*, 107–124. https://doi.org/10.1016/j.addr.2017.11.002
26. Silverthorn, D. U. (2007). *Human physiology: An integrated approach* (pp. 617–646). Pearson.
27. Palmer, K. L., Mashburn, L. M., Singh, P. K., & Whiteley, M. (2005). Cystic fibrosis sputum supports growth and cues key aspects of *Pseudomonas aeruginosa* physiology. *Journal of Bacteriology, 187*, 5267–5277. https://doi.org/10.1128/JB.187.15.5267-5277.2005
28. Guffey, J. S., & Wilborn, J. (2006). Effects of combined 405-nm and 880-nm light on *Staphylococcus aureus* and *Pseudomonas aeruginosa* in vitro. *Photomedicine and Laser Surgery, 24*, 680–683. https://doi.org/10.1089/pho.2006.24.680
29. Rompf, A., et al. (1998). Regulation of *Pseudomonas aeruginosa* hemF and hemN by the dual action of the redox response regulators Anr and Dnr. *Molecular Microbiology, 29*, 985–997. https://doi.org/10.1046/j.1365-2958.1998.00980.x
30. Doss, M., & Philipp-Dormston, W. K. (1971). Excretion of porphyrins by bacteria. *Experientia, 27*, 376–377. https://doi.org/10.1007/BF02137256
31. Ciofu, O., Hansen, C. R., & Høiby, N. (2013). Respiratory bacterial infections in cystic fibrosis. *Current Opinion in Pulmonary Medicine, 19*(3), 251–258.
32. Flemming, H. C., & Wingender, J. (2010). The biofilm matrix. *Nature Reviews Microbiology, 8*, 623–633. https://doi.org/10.1038/nrmicro2415
33. Giovannetti, R., Bartocci, V., Pucciarelli, F., & Petetta, L. (2008). Remarks on the reactions of a tetracarboxylic porphyrin with gold and silver ions: A spectrophotometric, TEM and SEM study. *Polyhedron, 27*, 1047–1053. https://doi.org/10.1016/j.poly.2007.11.040
34. Matošević, D., Tarle, Z., Miljanić, S., Meić, Z., Pichler, L., & Pichler, G. (2010). The detection of carious lesion porphyrins using violet laser induced fluorescence. *Acta stomatologica croatica, 44*, 232–240.
35. Bodelón, G., et al. (2016). Detection and imaging of quorum sensing in *Pseudomonas aeruginosa* biofilm communities by surface-enhanced resonance Raman scattering. *Nature Materials, 15*(11), 1203–1211. https://doi.org/10.1038/nmat4720
36. Bernstein, P. S., Delori, F. C., Richer, S., van Kuijk, F. J. M., & Wenzel, A. J. (2010). The value of measurement of macular carotenoid pigment optical densities and distributions in age-related macular degeneration and other retinal disorders. *Vision Research, 50*, 716–728. https://doi.org/10.1016/j.visres.2009.10.014
37. Ridley, C., & Thornton, D. J. (2018). Mucins: The frontline defence of the lung. *Biochemical Society Transactions, 46*, 1099–1106. https://doi.org/10.1042/BST20170402
38. Kiedrowski, M. R., et al. (2018). *Staphylococcus aureus* biofilm growth on cystic fibrosis airway epithelial cells is enhanced during respiratory syncytial virus coinfection. *mSphere, 3*, 1–17. https://doi.org/10.1128/msphere.00341-18
39. Flock, S. T., Jacques, S. L., Wilson, B. C., Star, W. M., & van Gemert, M. J. C. (1992). Optical properties of intralipid: A phantom medium for light propagation studies. *Lasers in Surgery and Medicine 12*, 510–519. https://doi.org/10.1002/lsm.1900120510
40. Hecht, E., & Zajac, A. (2003). *Optics*, 4th edn. (p. 50). Addison Wesley.
41. Fernandez, J. M., Bilgin, M. D., & Grossweiner, L. I. (1997). Singlet oxygen generation by photodynamic agents. *Journal of Photochemistry and Photobiology B: Biology. 37*, 131–140. https://doi.org/10.1016/S1011-1344(96)07349-6
42. Jacques, S. L., & Wang, L. (1995). Monte Carlo modeling of light transport in tissues. *Optical Response Laser-Irradiated Tissue, 2607*, 73–100. https://doi.org/10.1007/978-1-4757-6092-7_4
43. Beek, J. F., et al. (1997). The optical properties of lung as a function of respiration. *Physics in Medicine & Biology, 42*, 2263.

44. Lust, M. R. (2007). The pulmonary system. In S. J. Jenna & D. B. Bylund (Eds.), *xPharm: the comprehensive pharmacology reference* (pp. 1–6). Elsevier.
45. Jacques, S. L. (1992). Simple optical theory for light dosimetry during PDT. *Optical Methods Tumor Treatment and Detection: Mechanisms Techniques Photodynamic Therapy, 1645*, 155–165. https://doi.org/10.1117/12.60938
46. Morris, D. P. (2009). Optical properties of water. In G. E. Likens (Ed.), *Encyclopedia of inland waters* (pp. 682–689). Academic Press. https://doi.org/10.1016/B978-012370626-3.00069-7.
47. Balabushevich, N. G., Sholina, E. A., Mikhalchik, E. V., Filatova, L. Y., Vikulina, A. S., & Volodkin, D. (2018). Self-assembled mucin-containing microcarriers via hard templating on CaCO3 crystals. *Micromachines, 9*, 1–16. https://doi.org/10.3390/mi9060307